Black Sea Journal of Engineering and Science
doi: 10.34248/bsengineering.1640219

Open Access Journal
e-ISSN: 2619 - 8991

Research Article
Volume 8 - Issue 3: 715-728 / May 2025

IN SILICO EXPLORATION OF PLANT EXTRACTS AS ACHE INHIBITORS: INSIGHTS FROM MOLECULAR DYNAMICS AND MM/GBSA ANALYSIS FOR ALZHEIMER'S DRUG DEVELOPMENT

Barış KURT[1]*, Murat EVCİL[2], Ayşe BARAN[3]

[1]*Muş Alparslan University Faculty of Arts and Sciences, Department of Chemistry, 49000, Muş, Türkiye*
[2]*Dicle University Institute of Science and Technology, Department of Chemistry, 21280, Diyarbakir, Türkiye*
[3]*Mardin Artuklu University Graduate Education Institute, Department of Biology, 47200, Mardin, Türkiye*

Abstract: Alzheimer's disease is a long-term neurological disorder that affects memory and other cognitive abilities. Physostigmine is a drug still used in treating symptoms associated with this disease, with its primary mechanism of action being AChE inhibition. AChE plays a crucial role in cholinergic neurotransmission, and its inhibition has been linked to the improvement of symptoms in Alzheimer's disease. In this study, 34 phytochemicals detected through LC-MS/MS analysis of 13 plant species were investigated as potential alternative drug candidates to physostigmine. For this purpose, docking studies followed by molecular dynamics simulations and MM/GBSA energy calculations were performed. The results revealed that 24 out of 34 phytochemicals were either very close to physostigmine (MM/GBSA binding affinity: -26.102 kcal/mol) or better AChE inhibitors. Additionally, it was determined that physostigmine increased the flexibility of the molecule when bound to the AChE enzyme, a unique result compared to our drug candidates. Our research emphasizes the potential of plant-derived compounds as AChE inhibitors and presents promising candidates for future drug development studies. Furthermore, physostigmine's property of increasing enzyme flexibility offers a new perspective in drug design and indicates that the role of this feature in therapeutic efficacy needs to be examined in more detail.
Anahtar kelimeler: Medicinal plants, MM/GBSA, In silico, Drug development

Keywords: Medicinal plants, MM/GBSA, In silico, Drug development

***Corresponding author:** Muş Alparslan University Faculty of Arts and Sciences, Department of Chemistry, 49000, Muş, Türkiye
E mail: b.kurt@alparslan.edu.tr (B. KURT)
Barış KURT https://orcid.org/0000-0002-1406-0915
Murat EVCİL https://orcid.org/0000-0002-4646-8042
Ayşe BARAN https://orcid.org/0000-0002-2317-0489
Received: February 14, 2025
Accepted: March 21, 2025
Published: May 15, 2025

Cite as: Kurt B, Evcil M, Baran A. 2025. In silico exploration of plant extracts as AChE Inhibitors: İnsights from molecular dynamics and MM/GBSA analysis for Alzheimer's drug development BSJ Eng Sci, 8(3): 715-728.

1. Introduction

Acetylcholinesterase (AChE) plays a pivotal role in the cholinergic system of the central nervous system by terminating acetylcholine-mediated neurotransmission. Inhibition of AChE has been a target in treating neurodegenerative diseases due to its involvement in the pathogenesis of conditions such as Alzheimer's disease (AD) (Dorronsoro et al., 2003). Zimmerman & Soreq, (2006). AChE inhibitors are used to increase the concentration of acetylcholine in the synaptic cleft, enhancing cholinergic transmission and mitigating symptoms of AD. Notably, research highlights the multifaceted nature of neurodegenerative diseases, emphasizing the necessity for drugs that target various aspects of these conditions simultaneously (Kabir et al., 2019). Lustoza Rodrigues et al. (2023). The development of AChE inhibitors, including tacrine-based compounds, has shown promise in addressing the complex, multifactorial nature of AD, underscoring the ongoing need for innovative treatments that can slow disease progression and improve the quality of life for affected individuals (Bortolami et al., 2021).

In addition to Alzheimer's disease, AChE inhibitors play a critical role in the treatment of various other medical conditions, highlighting their broad therapeutic potential. For instance, Myasthenia Gravis (MG), a chronic autoimmune neuromuscular disorder characterized by weakness and rapid fatigue of the voluntary muscles, benefits from AChE inhibitors. These inhibitors are used to increase neuromuscular transmission and improve muscle strength by preventing the breakdown of acetylcholine at the neuromuscular junction, offering symptomatic relief to patients with MG (Punga & Stålberg, 2009). Mantegazza et al. (2020). Beyond neurological disorders, the modulation of AChE activity by certain glucans suggests a therapeutic pathway for diseases where the cholinergic system plays a part in the pathophysiology (Reale & Costantini, 2021). Benfante et al, (2021). However, the application of AChE inhibitors extends beyond these specific conditions, as ongoing research continues to uncover their utility in treating a spectrum of diseases where cholinergic dysfunction is implicated. This expanding role of AChE inhibitors underscores the importance of these compounds in

This work is licensed (CC BY-NC 4.0) under Creative Commons Attribution 4.0 International License

modern pharmacotherapy, offering hope for more effective treatments for a range of disorders beyond their traditional applications (Mukherjee et al., 2007). Walczak-Nowicka & Herbet (2021).

The search for new AChE inhibitors has led to a focus on plant-derived compounds, which offer a diverse range of potential therapeutic benefits (Howes et al., 2003). Huang et al. (2013). Murray et al. (2013). Ranjan & Kumari (2017). Alkaloids and certain meroterpenoids from fungi have shown strong AChE inhibitory activity, suggesting their potential in treating neurodegenerative disorders (Huang et al., 2013). Plant-derived compounds, including alkaloids, coumarins, flavonoids, and stilbenes, have also been identified as promising AChE inhibitors (Murray et al., 2013). These compounds have the potential to address the cholinergic deficit in Alzheimer's disease and other neurodegenerative disorders (Ranjan & Kumari, 2017). The exploration of these natural compounds not only contributes to our understanding of their biological activities but also supports the development of new therapeutic agents (Howes et al., 2003). Mukherjee et al., (2007).

Physostigmine is a drug used in the treatment of Alzheimer's disease and known as a cholinesterase inhibitor (Hampel et al., 2018). Although physostigmine does not permanently cure Alzheimer's disease, it is known to alleviate symptoms and slow the progression of the disease (Jenike et al., 1990). Coelho & Birks, (2001). There are studies on the positive effects of this drug on memory loss, which is one of the most important symptoms of the disease (Thal et al., 1983). Therefore, comparing a potential drug candidate with physostigmine will give an idea about the effectiveness of the drug.

This study aimed to discover new AChE inhibitors that could be used in the treatment of Alzheimer's disease. For this purpose, docking studies supported by molecular dynamics simulation and MM/GBSA analyses were conducted to determine the AChE enzyme inhibition potential of molecules derived from selected plant extracts. It was shown that molecules such as Epigallocatechin, Hesperidin, and Rutin could effectively inhibit this enzyme by binding to AChE with high binding affinity, and the potential of drug candidates was compared with physostigmine, which is used as an Alzheimer's drug in the market. The results reveal that the candidate molecules are very strong cholinesterase inhibitors and also show that the drug called physostigmine, which exhibits weaker binding activity compared to our candidate molecules, contributes to the flexibility of the protein during molecular dynamics simulation.

The results of this research represent an important step in the drug development process for the treatment of Alzheimer's disease. Detailed examination of the interactions between selected molecules and AChE will provide a better understanding of their potential effects on the disease mechanism. Moreover, our study is important in showing that plant-derived molecules can be considered as new drug candidates for the treatment of Alzheimer's disease. While all 34 different chemical compounds obtained from plant extracts had docking scores of -5.7 or lower, MM/GBSA calculations performed for 24 molecules showing better binding scores than -7.0 kcal showed that all molecules are potential drug candidates. Therefore, the effectiveness of plant-based drugs in Alzheimer's treatment has been theoretically proven through this study. In light of these findings, it is of great importance to evaluate these molecules not only for Alzheimer's disease but also for myasthenia gravis or glucan-related disorders targeting AChE inhibition in future studies. Further investigation of these candidate molecules through preclinical and clinical studies may contribute to the development of new and effective approaches for the treatment of these diseases.

2. Materials and Methods

2.1. Material

Between March and October 2023, parts of certain plants (leaves, flowers, seeds, and above-ground parts) were commercially purchased from various local markets, and their extracts were obtained. Their chemical compositions and contents were then analyzed using LC-MS/MS (Table 1).

2.2 Extraction process and determination of chemical compositions

The 15-gram powdered plant samples were taken in a glass flask and extracted in a magnetic stirrer with 300 ml of methanol at a constant stirring rate of 250 rpm. This process was repeated three times.

The obtained extracts underwent the evaporation process after having undergone the filtrating (Watman No. 1 filter) process and the crude extracts were obtained. 1 mg/mL of crude extracts were dissolved in methanol for LC-MS/MS analysis. Before LC-ESI/MS analysis, the solution was transferred to a vial and filtered using a 0.22 mm filter. For chromatographic separation, a Poroshell 120 EC-C18 column (100 mm, 4.6 mm I.D., 2.7 mm) was used. The filtered plant mixture was moved down the column by a carrier phase made of 0.1% formic acid and a mobile phase made of 5 mM ammonium formate. Mobile phase B was also used, which was made up of 0.1% formic acid in methanol and 5 mM ammonium formate (Baran et al., 2023).

Table 1. Details of plant species used

Species	Used Parts	Locality
Mentha longifolia (L.) HUDSON	Leaf	Mardin/Local Market
Celtis tournefortii LAM.	Leaf	Mardin/Local Market
Elaeagnus angustifolia L.	Flower and Leaf	Mardin/Midyat Local Market
Morus rubra L.	Leaf	Diyarbakir/Local Market
Pistacia eurycarpa L.	Leaf	Mardin/Local Market
Thymus fallax	Leaf	Mardin/Local Market
Gundelia tournefortii L.	Above ground parts	Diyarbakir/Local Market
Foeniculum vulgare MILLER	Seed	Diyarbakir/Local Market
Cucurbita moschata L.	Leaf	Diyarbakir/Local Market

2.3. Selecting potential Drug Candidate Molecules:

Among potential treatment approaches for Alzheimer's disease, the inhibition of AChE enzyme emerges as a significant strategy. In this context, molecules derived from natural sources attract attention as innovative drug candidates. Our research aims to discover new AChE inhibitors that could be used in the treatment of Alzheimer's disease. To achieve this, we first concentrated on extracts from a variety of botanical sources, such as the following: Mentha longifolia, Celtis tournefortii, Elaeagnus angustifolia, Morus rubra, Pistacia eurycarpa, Thymus fallax, Gundelia tournefortii, Foeniculum vulgare and Cucurbita moschata. These plants may have AChE inhibitory action and are commonly used in folk medicine to treat a variety of illnesses.

The first phase of our research involved a comprehensive biochemical analysis of the selected botanical extracts, utilizing Gas Chromatography-Mass Spectrometry (GC-MS) technology. This analysis enabled the detailed identification of active compounds within the extracts. The results revealed that each botanical extract contains rich and diverse molecular structures. The data obtained have been summarized in Table 2, listing each botanical extract and the identified active molecules in detail. All molecules selected for further study are based on these lists and are compounds naturally found in plants. The selected molecules were then subjected to a two-stage testing process. The first stage involved molecular docking in a computational environment. This method was used to assess the potential interaction mechanisms and binding affinities of the molecules with the AChE enzyme. The docking results demonstrated the interaction potentials and inhibition strengths of the molecules with AChE.

The second stage was molecular dynamics (MD) analysis, conducted to examine the stability and dynamic behavior of the molecule-enzyme complexes over time. Based on the docking results, the MD analysis allowed us to evaluate how effective and stable the selected molecules are in a biological environment. This two-pronged approach has guided us in identifying potential AChE inhibitors that could be used in the treatment of Alzheimer's disease. As a result of our research, a list of promising molecules derived from specific plant extracts and exhibiting potential for AChE inhibition has been compiled. These molecules stand out as strong candidates for future preclinical and clinical studies.

2.4. Docking Analysis:

Docking analysis was conducted to theoretically elucidate the biological activity. For this purpose, Autodock Vina (Eberhardt et al., 2021) along with MGL TOOLS 1.5.6 (Morris et al., 2009) were utilized. The 3D mol files of the ligands were downloaded from the ChemSpider (Pence and Williams, 2010) and The Cambridge Structural Database (Groom et al., 2016), followed by optimization. The AChE protein was sourced from the RCSB Protein Data Bank (rcsb.org) (Berman, 2000) with PDB ID: 6O4W. Due to the size of the protein being larger than the maximum size of the Autodock Tools gridbox, the protein was divided into chains A and B using the Chimera (Pettersen et al., 2004) software, and the ligands and water molecules within each chain were removed. With Autodock Tools (Morris et al., 2009), polar hydrogens and Kollman charges were added separately to each chain of the protein, a grid box was generated, and the chains were saved as pdbqt files with charges. Subsequently, the ligands were converted to pdbqt files using the prepare_ligands4.py program and a written shell script, and Gasteiger charges were added.

Docking procedures were then initiated with vina. exe. Each ligand underwent separate docking processes with both the A and B chains. Upon completion of the docking process, the lowest score from each docking event for both chains A and B was taken as the basis, and the receptor-ligand interaction was visualized and analyzed in the Discovery Studio Visualizer (BIOVIA, 2019) program.

Table 2. Chemical profile data of used plants and docking score capacities

	Detected Components	Docking Score (kcal/mol)
Mentha longifolia (Leaf)	Protocatechuic acid	-6.50
	Chlorogenic acid	-10.0
	Hydroxybenzaldeyde	-5.80
	Caffeic Acid	-7.50
	p-coumaric acid	-7.20
	Salicylic Acid	-6.50
	Resveratrol	-9.20
	Trans-ferulic acid	-7.30
	Scutellarin	-9.90
	Rutin	-11.4
	Naringenin	-8.40
Celtis tournefortii (Leaf)	Detected Components	
	Caffeic Acid	-7.50
	Vanillin	-6.00
	p-coumaric acid	-7.20
	Isoquercitrin	-8.50
	Quercetin	-9.50
Elaeagnus angustifolia (Fruit)	Detected Components	
	Gallic acid	-6.50
	Protocatechuic acid	-6.50
	Hydroxybenzaldeyde	-5.80
	p-coumaric acid	-7.20
Elaeagnus angustifolia (Flower)	Detected Components	
	p-coumaric acid	-7.20
	Trans-ferulic acid	-7.30
	Sinapic acid	-7.10
	Isoquercitrin	-8.50
	Kaempferol-3-glucoside	-8.20
	Fisetin	-8.90
	Trans-cinnamic acid	-7.10
	Naringenin	-8.40
Elaeagnus angustifolia (Leaf)	Detected Components	
	Vanillin	-6.00
	p-coumaric acid	-7.20
	Trans-ferulic acid	-7.30
	Rutin	-11.4
	Kaempferol-3-glucoside	-8.20
	Fisetin	-8.90
Morus rubra (Leaf)	Detected Components	
	Gallic acid	-6.50
	Protocatechuic acid	-6.50
	Chlorogenic acid	-10.0
	Hydroxybenzaldeyde	-5.80
	p-coumaric acid	-7.20
	Hesperidin	-10.8
	Isoquercitrin	-8.50

Table 2. Chemical profile data of used plants and docking score capacities (continued)

	Detected Components	Docking Score (kcal/mol)
	Shikimic acid	-6.10
	Gallic acid	-6.50
	Protocatechuic acid	-6.50
	Epigallocatechin	-7.40
	Catechin	-9.20
	Caffeic Acid	-7.50
	Vanillin	-6.00
Pistacia eurycarpa (Leaf)	*p*-coumaric acid	-7.20
	Salicylic Acid	-6.50
	Protocatehuic ethyl ester	-6.50
	Hesperidin	-10.8
	Isoquercitrin	-8.50
	Kaempferol-3-glucoside	-8.20
	Trans-cinnamic acid	-7.10
	Quercetin	-9.50
	Naringenin	-8.40
	Detected Components	
	Gallic acid	-6.50
	Chlorogenic acid	-10.0
	Hydroxybenzaldeyde	-5.80
	Caffeic Acid	-7.50
	Syringic acid	-6.50
	Vanillin	-6.00
Thymus fallax (Leaf)	*p*-coumaric acid	-7.20
	Taxifolin	-8.80
	Trans-ferulic acid	-7.30
	Scutellarin	-9.90
	Trans-cinnamic acid	-7.10
	Quercetin	-9.50
	Naringenin	-8.40
	Biochanin A	-9.80
	Detected Components	
	Protocatechuic acid	-6.50
Gundelia tournefortii (Leaf)	*p*-coumaric acid	-7.20
	Coumarin	-7.30
	Trans-cinnamic acid	-7.10
	Detected Components	
	Protocatechuic acid	-6.50
	Chlorogenic acid	-10.0
	Hydroxybenzaldeyde	-5.80
	Vanillic acid	-6.40
Foeniculum vulgare (Seed)	Caffeic Acid	-7.50
	Vanillin	-6.00
	p-coumaric acid	-7.20
	Trans-ferulic acid	-7.30
	Isoquercitrin	-8.50
	Kaempferol-3-glucoside	-8.20
	Detected Components	
	Protocatechuic acid	-6.50
Cucurbita moschata (Leaf)	Hydroxybenzaldeyde	-5.80
	Caffeine	-5.70
	p-coumaric acid	-7.20

2.5. Molecular Dynamics Simulation and MM/GBSA Calculations:

Following the completion of the docking process with Autodock, where 24 ligands exhibited binding energies superior to -7.0 kcal/mol, molecular dynamics simulations were initiated. The preparation of simulation files was conducted using the tleap program within the Amber22 suite, employing ff19SB force fields for the protein and gaff2 for the ligands. The simulation environment was constituted by an OPCBOX water box with a 10 Å edge length, incorporating OPC water molecules. The OpenMM 7 software (Eastman et al., 2017) facilitated the execution of the molecular dynamics simulation process, utilizing Nvidia Tesla A100 80 GB GPUs leased from Google Cloud for computational resources.

To expedite the simulation process, following the generation of topology and coordinate files, a "hydrogen mass repartitioning" procedure was implemented using the parmed program with the hmassrepartition command in parmed program (Hopkins et al., 2015). Case et al. (2023). Subsequently, a two-phase minimization protocol was initiated. In the initial phase, the complex was constrained with a force constant of 500 kcal/mol·Å^2, while water molecules were minimized over 1000 steps using the Particle Mesh Ewald (PME) method with a 10Å cutoff. The second phase involved removing the force constant from the complex and minimizing the entire system using the same method, but with an increased cutoff of 12Å.

The heating process was then initiated employing the Langevin thermostat and the SHAKE algorithm, maintaining a 12Å cutoff. The temperature was gradually increased to 298K in 1-degree increments. Upon reaching 298K, molecular dynamics simulation was conducted under 1 atm pressure, with a 4 ps relaxation time, utilizing the same thermostat and algorithm.

For rapid calculation of MM/GBSA energies during the preliminary trial, a 2 ns test was performed. Subsequently, the simulation was extended to 20 ns for molecules Hesperidin, Rutin, Chlorogenic acid, and Epigallocatechin, which exhibited the highest binding energies to Chain A, along with the Physostigmine molecule. As elaborated below, upon confirming the stability of RMSD values, it was determined that the simulation duration was sufficient, and the process was terminated.

This methodological approach ensures a comprehensive exploration of the system's conformational space while maintaining computational efficiency. The use of hydrogen mass repartitioning and the two-step minimization process allows for a more stable simulation environment. The gradual heating and equilibration phases, followed by the production run, provide a robust framework for analyzing the molecular interactions and dynamics of the studied compounds. The extension of the simulation to 20 ns for selected molecules offers valuable insights into their long-term behavior and binding characteristics, particularly in comparison to the known inhibitor, physostigmine. The stability of RMSD values serves as a critical indicator of simulation convergence, validating the adequacy of the chosen simulation duration for capturing relevant molecular events.

Additionally, the simulation phases were documented by generating output files in NetCDF format and saving checkpoint files at specified intervals. Upon the conclusion of the simulations, the ante-MMPBSA method was employed to generate prmtop files for the complex, ligand, and receptor, facilitating the computation of the binding energies of ligands to the receptor through MM/GBSA calculations. This process enabled a comprehensive analysis of the results from the molecular dynamics simulations and provided an assessment of the thermodynamic stability of the structures obtained during the simulation.

3. Result and Discussion

3.1. Docking Scores:

The results from the docking analysis are presented in Table 3. Among the evaluated molecules, Rutin, Hesperidin, Luteolin, and Chlorogenic acid exhibit the most pronounced binding energies. The docking scores for these compounds were determined to be -11.4, -10.0, -10.0, and -10.0 kcal/mol, respectively. These energy values indicate that these molecules bind to the receptor with a high affinity. Other compounds listed in the table generally possess binding energies of -6.0 or more negative scores (Kurt et al., 2020). Kurt (2022). Upon a detailed analysis, it was discerned that Rutin, which has the lowest (the best) docking score, establishes pi-donor hydrogen bonds with TYR:334 and PHE:335 on the A chain, engages in a pi alkyl interaction with LEU:73, and forms conventional hydrogen bonds with ARG:293, PHE:292, TYR:338,121,69 THR:72, and SER:290. This multitude of interactions signifies that the molecule binds to the chain with considerable stability (Figure 1).

When the same analysis was conducted for hesperidin, it was observed that the molecule forms a hydrogen bond with PHE:292 and a carbon-hydrogen bond with SER:200 on the A chain of the AChE protein. These interactions appear to be sufficient for the molecule to bind robustly to the protein (Figure 2).

Another compound demonstrating the highest docking score, Luteolin, was found to bind to the protein through the A chain via hydrogen bonds from PHE:292, GLY:119, and SER:200, and through a Pi-Sigma bond from TYR:338 (Figure 3).

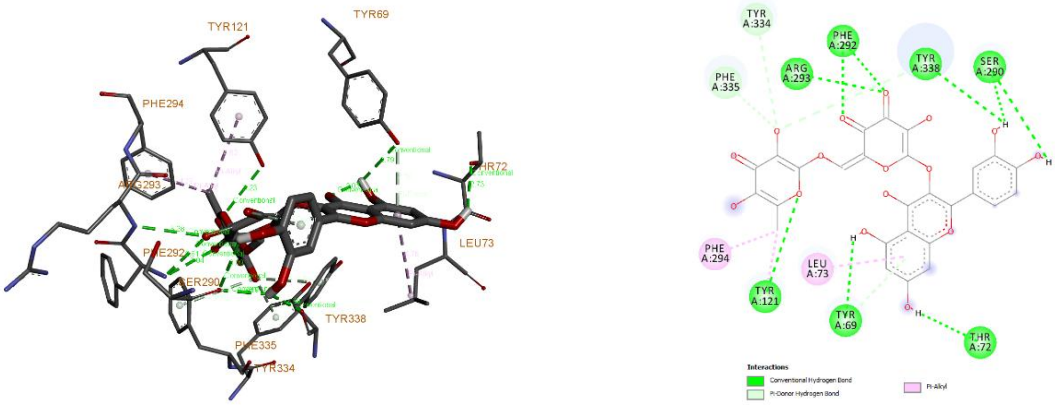

Figure 1. Docking interaction of Rutin with AChE-A Chain in 3D (left) and 2D (right).

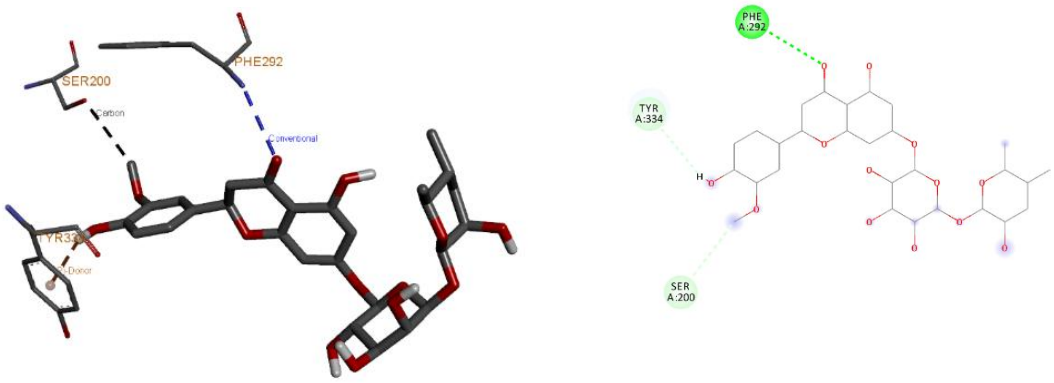

Figure 2. Docking interaction of Hesperidin with AChE-A Chain in 3D (left) and 2D (right).

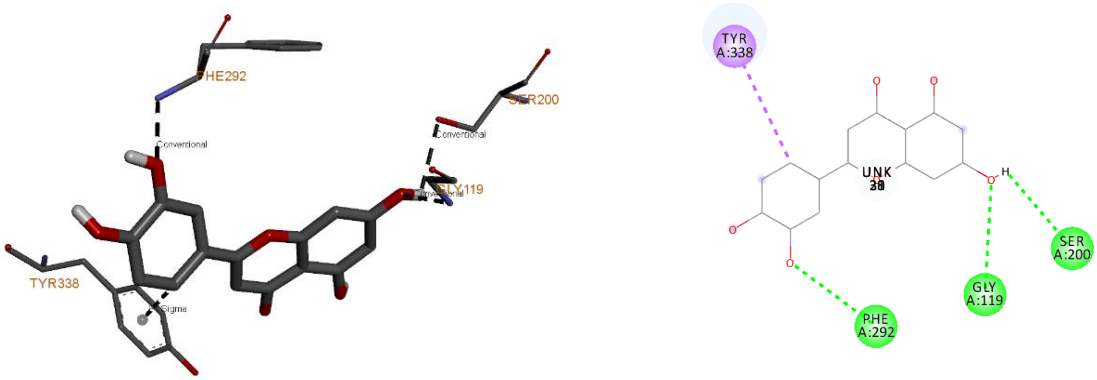

Figure 3. Docking interaction of Luteolin with AChE-A Chain in 3D (left) and 2D (right).

Figure 4 illustrates the docking interaction of Chlorogenic acid with the AChE-A Chain, presented in both 3D (left) and 2D (right) representations. The 3D model on the left offers a spatial view of how Chlorogenic acid fits into the binding pocket of the AChE-A Chain, while the 2D diagram on the right provides a simplified representation of the key interactions. In the 3D model, we can observe the complex structure of Chlorogenic acid (shown in black) situated within the protein binding site. The amino acid residues involved in the interaction are depicted as stick models, with different colors representing various elements.

The 2D diagram elucidates the specific interactions between Chlorogenic acid and the protein residues: Pi-Sigma interactions are observed with PHE335 and TYR334, indicated by pink dashed lines. These interactions contribute to the stability of the binding. A hydrogen bond is formed with TRP83, shown by a purple dashed line. This bond likely plays a crucial role in anchoring the compound within the binding site. Several other amino acid residues are highlighted in green (e.g., ASP71, TYR121, TYR338, PHE294, PHE292, VAL291), suggesting their proximity to the binding site and potential involvement in creating a favorable binding environment. ARG293 is specifically labeled, indicating its importance in the binding interaction. The "Carbon pi-

H" notation suggests a possible pi-hydrogen interaction with this residue. The purple-colored residues (TRP83, HIS444) appear to be involved in key interactions, possibly through aromatic or electrostatic contributions. This detailed visualization of the docking interaction provides valuable insights into the molecular basis of Chlorogenic acid's binding to the AChE-A Chain, which could be crucial for understanding its potential pharmacological effects or for guiding future drug design efforts targeting this protein.

The binding sites and interactions of the remaining ligands with the protein are presented in Table 3 and Figure 5. Based on the data in the table, it can be posited that all evaluated molecules have potential as effective inhibitors for AChE. The table also suggests that binding predominantly occurs through the A chain, highlighting its significance in drug targeting.

Following the binding analyses in Table 3, attempts were made to statistically identify the most active regions in chains A and B. For this purpose, a Python program was prepared that counts each binding site in Table 3 individually. The results from the program can be seen in Table 4. Accordingly, the protein regions that interacted most with the ligands were TRY A:121, PHE A:292, TYR A:334, SER A:290, and GLU A:299 in chain A. The active region in chain B is significantly smaller compared to chain A.

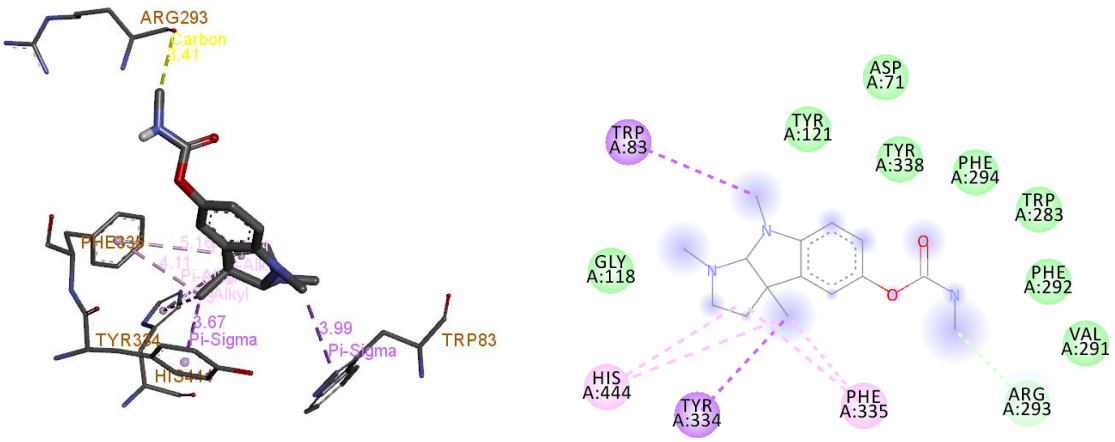

Figure 4. Docking interaction of Chlorogenic acid with AChE-A Chain in 3D (left) and 2D (right).

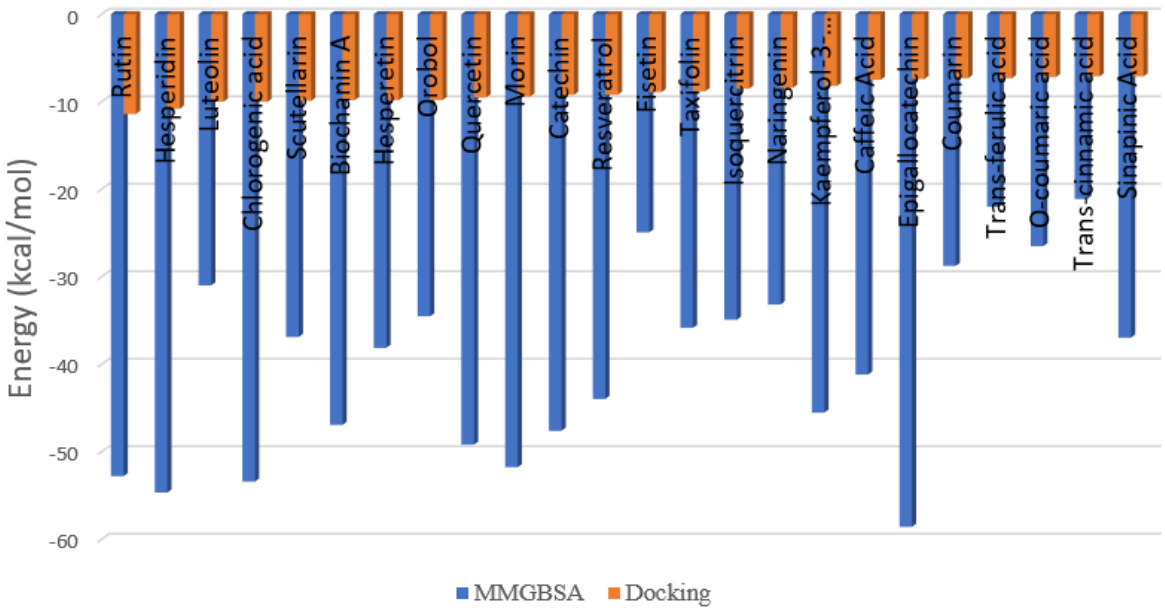

Figure 5. Docking Score and MM/GBSA energy of 24 selected molecules.

Table 3. Binding energies of the ligands to which the docking process was applied. Since the AChE molecule is two-chained, the docking process was applied separately for each chain, and the one with the lower energy was considered as the primary

Compund	Chain-a	Chain-b	Docking Score	Binding Chain	MM/GBSA Energy (kcal/mol)	Binding Sides
Rutin	-11.4	-10.7	-11.4	chain a	-52.792	pi-donor: TYR A: 334, PHE A: 335; hyrogen bond(s): ARG A: 293, PHE A: 292, TYR A: 338,121,69 THR A: 72, and SER A: 290
Physostigmine*	-8.30	-7.30	-8.30	chain a	-26.102*	vdw:ASP A:71 TYR A:338 PHE A:294 TRP A:283 GLY A:118 PHE A:292 VAL A:291 pi-sigma: TRP A:83 TYR A:334 pi-alkyl: HIS A:444 PHE A:335
Hesperidin	-10.8	-9.3	-10.8	chain a	-54.666	carbon-hydrogen bond:ARG A:293 hydrogen bond(s): PHE A: 292; carbon-hydrogen bond(s): SER A:200
Luteolin	-10	-10	-10	chain a	-30.993	hydrogen bond(s): PHE A :292, GLY A: 119, and SER A: 200; Pi-Sigma bond(s): TYR A: 338
Chlorogenic acid	-10	-6.8	-10	chain a	-53.408	pi-donor: SER A: 290, GLY A: 119, SER A: 200, TYR A: 121; Donor-donor: ARG A: 293; Pi donor: TYR A: 338
Scutellarin	-9.9	-9.2	-9.9	chain a	-36.892	hydrogen bond(s): TYR A:334, THR A: 72,ASP A: 71
Biochanin A	-9.8	-9.5	-9.8	chain a	-46.935	hydrogen bond(s): TYR A: 121, PHE A: 292; Pi-Donor: TYR A: 338;Pi-Sigma: TYR A :338
Hesperetin	-9.8	-8.9	-9.8	chain a	-38.127	hydrogen bond(s): SER A: 122,TYR A: 121, PHE A: 292, HIS A: 444; Carbon-Hydrogen Bonds: TYR A: 334, PHE A: 335; Pi-Sigma: TYR A: 83, TYR A: 338
Orobol	-9.1	-9.8	-9.8	cahin b	-34.515	hydrogen bond(s): HIS B: 824, GLN B:828
Quercetin	-9.5	-9.2	-9.5	chain a	-49.188	hydrogen bond(s): SER A: 290, ARG A:293, TYR A: 121
Morin	-9.2	-9.4	-9.4	cahin b	-51.763	hydrogen bond(s): SER B: 830, TYR B: 661, ASP B: 611
Catechin	-9.2	-9.2	-9.2	chain a	-47.607	donor-donor: PHE A: 292; pi-donor: TRP A: 283
Resveratrol	-9.2	-6.8	-9.2	chain a	-43.97	hydrogen bond(s): SER A: 290
Fisetin	-8.9	-6.9	-8.9	chain a	-24.935	hydrogen bond(s): SER A: 290, ARG A: 293, TYR A: 121, PHE A: 292
Taxifolin	-8.8	-8.7	-8.8	chain a	-35.834	hydrogen bond(s): SER A: 290, TYR A:121, PHE A: 292, GLN A: 288; Pi-Donor: TRP A: 283
Isoquercitrin	-8.5	-8.2	-8.5	chain a	-34.91	hydrogen bond(s): SER A: 290, TYR A :121, TYR A :338, PHE A:292, GLN A: 288; Pi-Donor: HIS A: 284, PHE A: 292; Carbon-Hydrogen: VAL A: 291
Naringenin	-8.4	-8.3	-8.4	chain a	-33.171	hydrogen bond(s): THR A: 72, TYR A: 121, PHE A:292
Kaempferol-3-glucoside	-8.1	-8.2	-8.2	cahin b	-45.531	hydrogen bond(s): PRO B: 772, THR B: 775; Carbon-Hydrogen Bonds: PRO B: 947,HIS B: 942,GLY B: 771
Caffeic Acid	-7.5	-5.7	-7.5	chain a	-41.171	hydrogen bond(s): GLU A: 199, TYR A: 334, TYR A: 338, ASP A: 71; Carbon-hydrogen bonds: THR A: 80, TRP A: 83
Epigallocatechin	-7.4	-6.7	-7.4	chain a	-58.583	hydrogen bond(s): SER A: 290, TYR A: 69
Coumarin	-7.3	-6.9	-7.3	chain a	-28.767	hydrogen bond(s): SER A: 200; Carbon-Hydrogen: HIS A:444
Trans-ferulic acid	-7.3	-7.3	-7.3	chain a	-22.007	hydrogen bond(s): ARG A: 293; Pi-donör: PYR A: 334
p-coumaric acid	-7.2	-7	-7.2	chain a	-26.51	hydrogen bond(s): TYR A: 121; Donor-donor: PHE A: 292

Table 3. Binding energies of the ligands to which the docking process was applied. Since the AChE molecule is two-chained, the docking process was applied separately for each chain, and the one with the lower energy was considered as the primary (contunied)

Compund	Chain-a	Chain-b	Docking Score	Binding Chain	MM/GBSA Energy (kcal/mol)	Binding Sides
Trans-cinnamic acid	-7.1	-7	-7.1	chain a	-21.109	hydrogen bond(s): TYR A: 334, TYR A: 338, ASP A: 71; Carbon-Hydrogen: TRP A: 83
Sinapinic Acid	-7.1	-6.5	-7.1	chain a	-36.974	hydrogen bond(s): GLU A: 199; Pi-Sigma: TYR A: 334; Carbon-hydrogen bonds: TYR A: 121, SER A: 122, TRP A: 83, GLY A: 445
Ethyl protocatechuate	-6.8	-6.8	-6.8	chain a		hydrogen bond(s): TYR A: 334, GLU A: 199; Pi-Donor: TRP A: 83;Pi-Sigma: PHE A: 335
Gallic acid	-6.4	-6.5	-6.5	cahin b		hydrogen bond(s): TYR B: 661, ASP B: 611; Pi Donor: TRP B:623
Protocatechuic acid	-6.5	-6.3	-6.5	chain a		hydrogen bond(s): TYR A: 130, GLU A: 199;Pi Donor: TRY A:334; Pi-Sigma: TRP A:83
Salicylic Acid	-6.5	-6.2	-6.5	chain a		hydrogen bond(s): TYR A: 121, ASP A: 71, TYR A: 338, TYR A: 334
Syringic acid	-6.5	-5.1	-6.5	chain a		hydrogen bond(s): SER A: 290, TYR A: 121, TYR A: 338, PHE A:292; Carbon-Hydrogen: VAL A: 291; Pi-Sigma: TRP A: 283
Vanillic acid	-6.4	-6	-6.4	chain a		hydrogen bond(s): TYR A: 121, TYR A: 338, PHE A: 292; Carbon-Hydrogen: VAL A: 291
Shikimic acid	-6.1	-5.6	-6.1	chain a		hydrogen bond(s): TYR A: 334, TYR A: 121, TYR A: 130, GLU A: 199; Pi-Donör: TRP A: 83
Vanillin	-6	-5.3	-6	chain a		hydrogen bond(s): PHE A: 292, TYR A: 338, TYR A: 121; Carbon-Hydrogen: VAL A: 291
Hydroxybenzaldeyde	-5.8	-5.7	-5.8	chain a		hydrogen bond(s): TYR A: 121, ARG A: 293, PHE A: 292
Caffeine	-5.7	-5.7	-5.7	chain a		hydrogen bond(s): ASP A: 371, TYR A: 334, TYR A: 338, GLU A: 199; Carbon-Hydrogen Bonds: THR A: 80, TRP A: 83

Table 4: Count of binding sites from Table 3. Based on this, TRY A:121 has interacted the most with the docked ligands

Chain A		Chain B	
Binding Side	Count	Bindin Side	Count
TYR A: 121	15	TYR B: 661	2
PHE A: 292	13	ASP B: 611	2
TYR A: 338	13	HIS B: 824	1
TYR A: 334	10	SER B: 830	1
SER A: 290	9	PRO B: 772	1
GLU A: 199	6	THR B: 775	1
TRP A: 83	6	PRO B: 947	1
ARG A: 293	5	HIS B: 942	1
ASP A: 71	5	GLY B: 771	1
VAL A: 291	5		

3.2. Active Sites

Table 4 displays the results of docking studies with AChE and identifies the amino acid residues where ligands most frequently bind on the enzyme. In CHAIN A, aromatic amino acid residues such as TYR A: 121, PHE A: 292, and TYR A: 338 are observed to be common ligand binding sites. This suggests that ligands may form strong π-π interactions and hydrophobic contacts with these aromatic surfaces. In CHAIN B, interactions with various amino acids occur less frequently, indicating that ligands exhibit fewer specific interactions on CHAIN B compared to CHAIN A. We believe these findings will provide a foundation for a more detailed characterization of AChE's active sites and binding regions.

3.3. Molecular Dynamics Simulation and MM/GBSA Results:

The analysis of docking scores and MM/GBSA binding energies in Table 3 reveals a high affinity of a range of compounds to AChE, with several exhibiting particularly strong binding preferences. Compounds like Rutin and Hesperidin not only show favorable interactions with aromatic residues within Chain A, indicative of potent π-π interactions, but also display consistently better MMGBSA binding energies, suggesting their potential as high-efficiency AChE inhibitors. This specificity, particularly in the hydrophobic pocket of Chain A, may account for the enhanced interaction strength, and the varied binding sites observed across the compounds emphasize the role of individual residue interactions in binding efficacy. Collectively, these insights offer a comprehensive foundation for advancing these compounds in the development of Alzheimer's disease therapeutics.

Initially, a 2 ns preliminary trial was conducted for all molecules with docking energies better than -7.0 kcal/mol. Figure 5 shows the docking scores and MM/GBSA binding energies for the 24 selected molecules. Following this stage, MMGBSA energies were calculated and Table 3 was created.

Based on the data in Table 3, the 4 molecules showing the best MMGBSA binding energy were selected and compared with physostigmine, the current Alzheimer's disease drug on the market. All 4 of these molecules exhibited better MMGBSA values than physostigmine.

Consequently, the molecular dynamics simulation times of the selected chemicals and physostigmine were extended to 20 ns for re-examination. RMSF (Figure 6) and RMSD (Figure 7) graphs were plotted to examine the stability of the simulations.

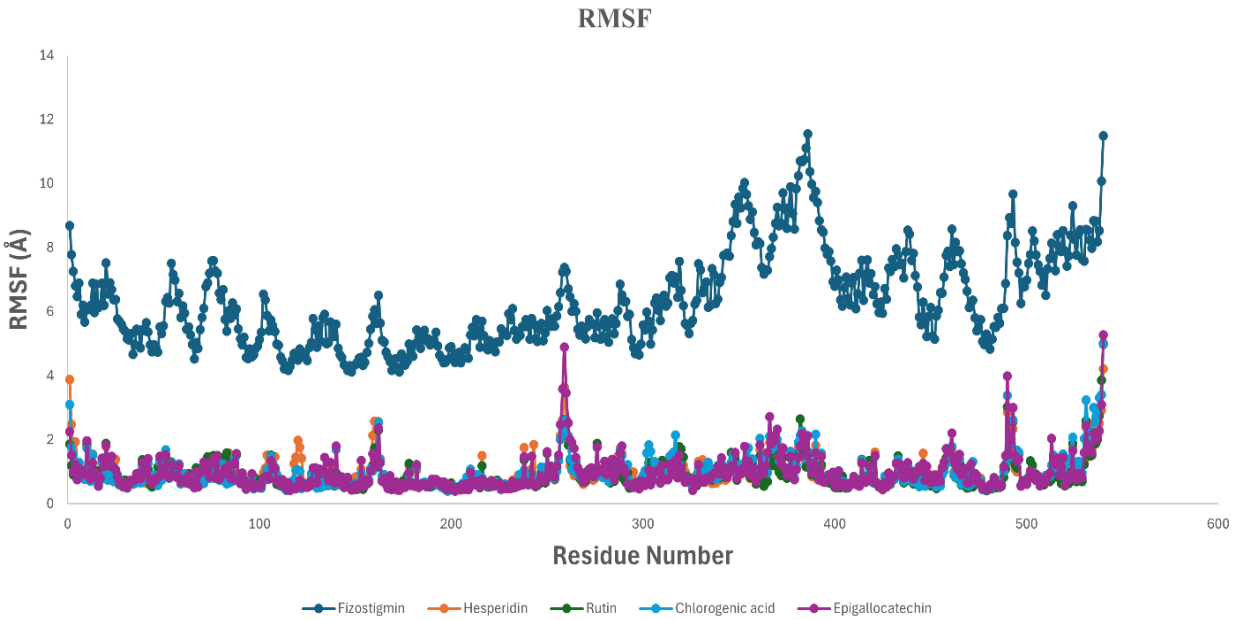

Figure 6. RMSF chart of Physostigmine, Hesperidin, Rutin, Chlorogenic acid, and Epigallocatechin.

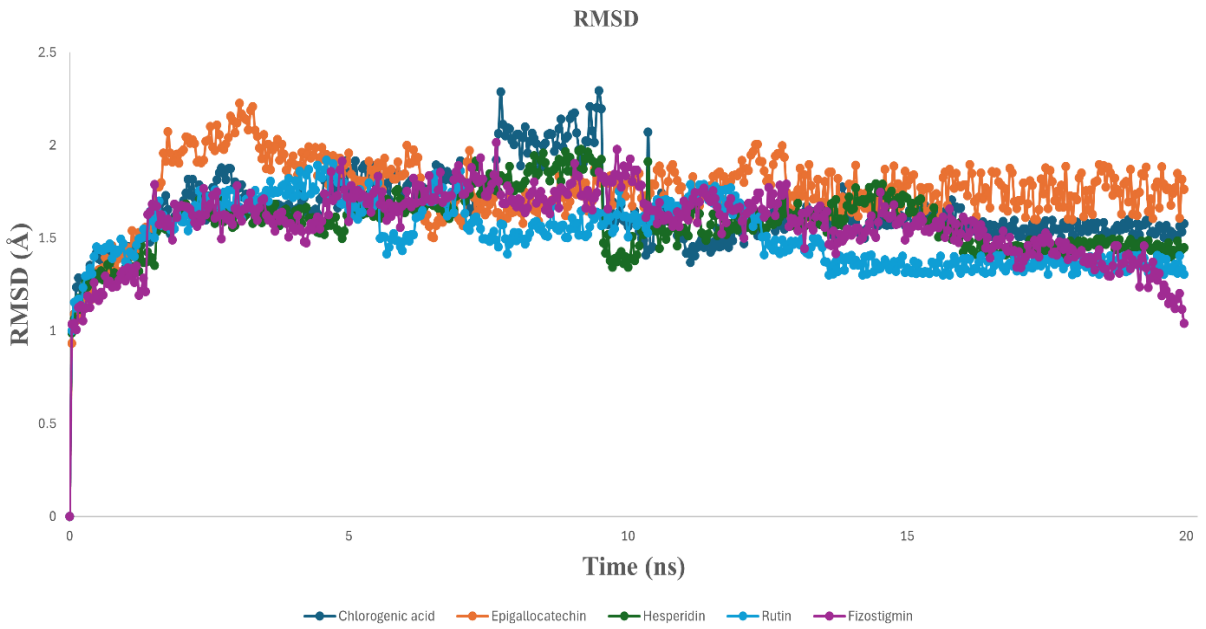

Figure 7. RMSD Chart of Physostigmine, Hesperidin, Rutin, Chlorogenic acid, and Epigallocatechin.

3.4. RMSF and RMSD

Figure 6 is an RMSF (Root Mean Square Fluctuation) analysis showing the behavior of five different components (Physostigmine, Hesperidin, Rutin, Chlorogenic acid, and Epigallocatechin) over time. RMSF is a frequently used measure in molecular dynamics simulations and indicates how much molecules or atoms deviate from their average positions. The graph shows atomic fluctuations between the 540-residue chain-A and ligands. Physostigmine exhibits generally higher RMSF values compared to other compounds, indicating that Physostigmine affects a wider region of the protein or shows more dynamic interactions. We can interpret this as physostigmine's binding being more flexible compared to other molecules.

For all components, significant peaks are observed especially in the 100-200 and 400-500 residue ranges. This indicates that these regions are more sensitive or flexible to ligand binding. Physostigmine significantly diverges from other compounds, especially in the 300-400 residue range. This suggests that Physostigmine shows a unique interaction in this region or significantly affects the conformation of this region.

Other compounds, Hesperidin, Rutin, Chlorogenic acid, and Epigallocatechin generally exhibit similar RMSF profiles. Among these molecules, Chlorogenic acid belongs to a phenolic acid group while the other 3 belong to the flavonoid group. This suggests that both phenolic acids and flavonoids may show similar effects, however, more detailed further studies focusing solely on this issue should be conducted to reach a definitive conclusion. All 4 molecules exhibited similar properties with minor differences.

Binding regions showing high RMSF values (e.g., 100-200 and 400-500 residue ranges) may indicate potential ligand binding regions. These regions may be flexible or adaptive parts where compounds interact.

Structural Stability: Regions showing low RMSF values (e.g., 0-100 and 200-300 residue ranges) may indicate more stable or rigid parts of the protein. These regions may be parts that maintain the structural integrity of the protein or are important for catalytic activity.

The RMSD (Root Mean Square Deviation) analysis in Figure 7 examines the structural changes of five different compounds (Chlorogenic acid, Epigallocatechin, Hesperidin, Rutin, and Physostigmine) over a 20-nanosecond molecular dynamics simulation. The analysis shows how the molecules deviate from their minimized initial geometries, and these changes can be interpreted as an indicator of the molecules' conformational dynamics.

All molecules show conformational changes at the start of the simulation. After approximately 5 nanoseconds (ns), RMSD values for most compounds reach a relatively stable plateau, fluctuating around 1.5 angstroms (Å). This indicates structural stability observed throughout the simulation. Epigallocatechin has the highest RMSD values, generally ranging between 1.7-2.0 Å. This suggests that Epigallocatechin undergoes more conformational changes compared to other components, thus exhibiting a more dynamic structure. Chlorogenic Acid, while generally following a stable course, shows a notable peak around 10 ns. This indicates that the molecule undergoes a temporary conformational change during a specific time period. Hesperidin and Rutin exhibit similar and relatively low RMSD profiles. Both molecules generally show a stable RMSD of 1.5 Å, indicating that they display relative structural consistency throughout the simulation. Physostigmine, on the other hand, shows a profile relatively different from the others: While initially exhibiting an RMSD profile similar to other molecules, a decrease in RMSD

values was observed in the final part of the simulation (between 15-20 ns). This decrease indicates that Physostigmine becomes structurally more stable in the later stages of the simulation.

4. Conclusion

In conclusion, the 20 ns simulation time appears to provide sufficient equilibration for all components studied. While Epigallocatechin exhibits a dynamic structure, other compounds generally show more stable structures. These differences are important for better understanding the functionality and interactions of molecules in biological systems.

This study aims to discover new AChE inhibitors that can be used in the treatment of Alzheimer's disease and to develop new, effective, and cost-efficient drugs that could serve as alternatives to physostigmine, which is currently used in treating Alzheimer's disase symptoms.

Molecules obtained from selected plant extracts have played a critical role in identifying candidate molecules with AChE enzyme inhibition potential. Docking studies, molecular dynamics simulations, and MM/GBSA analyses have demonstrated that these molecules can effectively inhibit this enzyme by binding to AChE with high affinity.

Author Contributions

The percentages of the authors' contributions are presented below. All authors reviewed and approved the final version of the manuscript.

	B.K.	M.E.	A.B.
C	40	30	30
D	40	30	30
S	40	30	30
DCP	40	30	30
DAI	40	30	30
L	40	30	30
W	40	30	30
CR	40	30	30
SR	40	30	30
PM	40	30	30

C=Concept, D= design, S= supervision, DCP= data collection and/or processing, DAI= data analysis and/or interpretation, L= literature search, W= writing, CR= critical review, SR= submission and revision, PM= project management

Conflict of Interest

Authors declare there is no conflict of interest

Ethical Consideration

Ethics committee approval was not required for this study because there was no study on animals or humans.

References

Baran MF, Keskin C, Baran A, Eftekhari A, Omarova S, Khalilov R, Atalar MN. 2023. The investigation of the chemical composition and applicability of gold nanoparticles synthesized with Amygdalus communis (almond) leaf aqueous extract as antimicrobial and anticancer agents. Molecules, 28(6): 2428. https://doi.org/10.3390/molecules28062428

Benfante R, Di Lascio S, Cardani S, Fornasari D. 2021. Acetylcholinesterase inhibitors targeting the cholinergic anti-inflammatory pathway: a new therapeutic perspective in aging-related disorders. Aging Clin Exp Res, 33(4): 823-834. https://doi.org/10.1007/s40520-019-01359-4

Berman HM. 2000. The protein data bank. Nucleic Acids Res, 28(1): 235-242. https://doi.org/10.1093/nar/28.1.235.

BIOVIA, 2019. Discovery studio visualizer. Dassault Systèmes, San Diego, CA, USA, pp:152.

Bortolami M, Rocco D, Messore A, Di Santo R, Costi R, Madia VN, Pandolfi F. 2021. Acetylcholinesterase inhibitors for the treatment of Alzheimer's disease - a patent review (2016-present). Expert Opin Ther Pat, 31(5): 399-420. https://doi.org/10.1080/13543776.2021.1874344

Case DA, Aktulga HM, Belfon K, Ben-Shalom IY, Berryman JT, Brozell SR, Xiong Y. 2023. AMBER 2023. University of California, San Francisco, CA, USA, pp: 32.

Coelho Filho JM, Birks J. 2001. Physostigmine for dementia due to Alzheimer's disease. Cochrane Database Syst Rev, 2001(2): CD001499. https://doi.org/10.1002/14651858.CD001499

Dorronsoro I, Castro A, Martinez A. 2003. Peripheral and dual binding site inhibitors of acetylcholinesterase as neurodegenerative disease modifying agents. Expert Opin Ther Pat, 13(11): 1725-1732. https://doi.org/10.1517/13543776.13.11.1725

Eastman P, Swails J, Chodera JD, McGibbon RT, Zhao Y, Beauchamp KA, Pande VS. 2017. OpenMM 7: rapid development of high performance algorithms for molecular dynamics. PLoS Comput Biol, 13(7): e1005659. https://doi.org/10.1371/journal.pcbi.1005659

Eberhardt J, Santos-Martins D, Tillack AF, Forli S. 2021. AutoDock Vina 1.2.0: new docking methods, expanded force field, and Python bindings. J Chem Inf Model, 61(8): 3891-3898. https://doi.org/10.1021/acs.jcim.1c00203

Groom CR, Bruno IJ, Lightfoot MP, Ward SC. 2016. The Cambridge structural database. Acta Crystallogr B, 72(2): 171-179. https://doi.org/10.1107/S2052520616003954

Hampel H, Mesulam MM, Cuello AC, Farlow MR, Giacobini E, Grossberg GT, Khachaturian ZS. 2018. The cholinergic system in the pathophysiology and treatment of Alzheimer's disease. Brain, 141(7): 1917-1933. https://doi.org/10.1093/brain/awy132

Hopkins CW, Le Grand S, Walker RC, Roitberg AE. 2015. Long-time-step molecular dynamics through hydrogen mass repartitioning. J Chem Theory Comput, 11(4): 1864-1874. https://doi.org/10.1021/ct5010406

Howes MR, Perry NSL, Houghton PJ. 2003. Plants with traditional uses and activities, relevant to the management of Alzheimer's disease and other cognitive disorders. Phytother Res, 17(1): 1-18. https://doi.org/10.1002/ptr.1280

Huang L, Su T, Li X. 2013. Natural products as sources of new lead compounds for the treatment of Alzheimer's disease. Curr Top Med Chem, 13(15): 1864-1878. https://doi.org/10.2174/15680266113139990142

Jenike MA, Albert M, Baer L, Gunther J. 1990. Oral physostigmine as treatment for primary degenerative dementia: a double-blind placebo-controlled inpatient trial. J

Geriatr Psychiatry Neurol, 3(1): 13-16. https://doi.org/10.1177/089198879000300104

Kabir MT, Uddin MS, Begum MM, Thangapandiyan S, Rahman MS, Aleya L, Ashraf GM. 2019. Cholinesterase inhibitors for Alzheimer's disease: multitargeting strategy based on anti-Alzheimer's drugs repositioning. Curr Pharm Des, 25(33): 3519-3535. https://doi.org/10.2174/1381612825666191008103141

Kurt B, Temel H, Atlan M, Kaya S. 2020. Synthesis, characterization, DNA interaction and docking studies of novel Schiff base ligand derived from 2,6-diaminopyridine and its complexes. J Mol Struct, 1209: 127928. https://doi.org/10.1016/j.molstruc.2020.127928

Kurt B. 2022. Investigation of the potential inhibitor effects of lycorine on SARS-CoV-2 main protease (Mpro) using molecular dynamics simulations and MMPBSA. Int J Life Sci Biotechnol, 5(3): 424-435. https://doi.org/10.38001/ijlsb.1110761

Lustoza Rodrigues TCM, de Sousa NF, dos Santos AMF, Aires Guimarães RD, Scotti MT, Scotti L. 2023. Challenges and discoveries in polypharmacology of neurodegenerative diseases. Curr Top Med Chem, 23(5): 349-370. https://doi.org/10.2174/1568026623666230126112628

Mantegazza R, Vanoli F, Frangiamore R, Cavalcante P. 2020. Complement inhibition for the treatment of myasthenia gravis. Immunotargets Ther, 9: 317-331. https://doi.org/10.2147/ITT.S261414

Morris GM, Huey R, Lindstrom W, Sanner MF, Belew RK, Goodsell DS, Olson AJ. 2009. AutoDock4 and AutoDockTools4: automated docking with selective receptor flexibility. J Comput Chem, 30(16): 2785-2791. https://doi.org/10.1002/jcc.21256

Mukherjee PK, Kumar V, Mal M, Houghton PJ. 2007. Acetylcholinesterase inhibitors from plants. Phytomedicine, 14(4): 289-300. https://doi.org/10.1016/j.phymed.2007.02.002

Murray A, Faraoni M, Castro M, Alza N, Cavallaro V. 2013. Natural AChE inhibitors from plants and their contribution to Alzheimer's disease therapy. Curr Neuropharmacol, 11(4): 388-413. https://doi.org/10.2174/1570159X11311040004

Pence HE, Williams A. 2010. ChemSpider: an online chemical information resource. J Chem Educ, 87(11): 1123-1124. https://doi.org/10.1021/ed100697w

Pettersen EF, Goddard TD, Huang CC, Couch GS, Greenblatt DM, Meng EC, Ferrin TE. 2004. UCSF Chimera: a visualization system for exploratory research and analysis. J Comput Chem, 25(13): 1605-1612. https://doi.org/10.1002/jcc.20084

Punga AR, Stålberg E. 2009. Acetylcholinesterase inhibitors in MG: to be or not to be? Muscle Nerve, 39(6): 724-728. https://doi.org/10.1002/mus.21319

Ranjan N, Kumari M. 2017. Acetylcholinesterase inhibition by medicinal plants: a review. Ann Plant Sci, 6(6): 1640. https://doi.org/10.21746/aps.2017.06.003

Reale M, Costantini E. 2021. Cholinergic modulation of the immune system in neuroinflammatory diseases. Diseases, 9(2): 29. https://doi.org/10.3390/diseases9020029

Thal LJ, Fuld PA, Masur DM, Sharpless NS. 1983. Oral physostigmine and lecithin improve memory in Alzheimer disease. Ann Neurol, 13(5): 491-496. https://doi.org/10.1002/ana.410130504

Walczak-Nowicka ŁJ, Herbet M. 2021. Acetylcholinesterase inhibitors in the treatment of neurodegenerative diseases and the role of acetylcholinesterase in their pathogenesis. Int J Mol Sci, 22(17): 9290. https://doi.org/10.3390/ijms22179290

Zimmerman G, Soreq H. 2006. Termination and beyond: acetylcholinesterase as a modulator of synaptic transmission. Cell Tissue Res, 326(2): 655-669. https://doi.org/10.1007/s00441-006-0239-8